

# Twisted electromagnetic sinc Schell-model beam and its transmission in a turbulent atmosphere

CHANGYOU ZHANG, WENYU FU\*

College of Artificial Intelligence, Jiang-Xi University of Engineering Xinyu,  
33800, Jiangxi, China

\*Corresponding author: qytcfwy@163.com

We present the twisted electromagnetic sinc-correlation Schell-model (EM TSSM) beam as an extension of the cylindrical sinc Schell-model beam and analyze the necessary source parameter conditions to generate a physically viable beam. Furthermore, we thoroughly investigate the propagation properties of the EM TSSM beam in atmospheric turbulence using the extended Huygens–Fresnel integral, explicitly focusing on spectral intensity, degree of polarization (DOP), and degree of coherence (DOC). It shows that the twisted phase has a noticeable impact on the intensity profiles of these beams, causing them to exhibit rotation and self-splitting while still maintaining their shape in free space. Moreover, during propagation through a turbulent atmosphere, it exhibits self-combining properties over a long range and recovers the plat-topped distribution. Compared with the sinc Schell-model beam without the twisted phase, the DOP distribution of such a beam can rotate around its distribution center. As these beams propagate through turbulent atmospheres, they can self-heal their DOP distribution within specific ranges affected by atmospheric turbulence. A twist factor causes non-unidirectional rotation of the DOC distribution in free space. The DOC gradually transforms from multi-strip profiles into a Gaussian-like distribution. Furthermore, the beam parameters play a crucial role in shaping the DOC. The results will be useful in optical trapping and optical communication.

Keywords: twisted, sinc Schell-model beam, beam propagation, atmospheric turbulence.

## 1. Introduction

The advantages of partially coherent beams over fully coherent beams have been widely recognized and supported by theoretical and experimental research [1-4]. Among the various types of partially coherent beams, extensive studies have been conducted on the Gaussian Schell-model beam with a uniform correlation structure, investigating their propagation properties in free space and random media [5-8]. As researchers sought to explore new possibilities, various beams with different shapes were introduced. The pioneering work of GORI *et al.* provided sufficient conditions for designing

genuine spatial correlation functions [9, 10]. A series of novel sources with non-conventional Gaussian correlation functions were developed by selecting diverse correlation functions, showcasing exceptional propagation characteristics such as self-shaping, self-splitting, and self-focusing in free space and random media [11-14]. Recently, MEI introduced two types of partially coherent beams utilizing the sinc Schell-model function [15]. These novel sources exhibit stable flat and dark hollow profiles in the far field, garnering significant interest among researchers. Subsequently, various beams related to the sinc Schell-model-correlated function have been extensively investigated, including cylindrical sinc Gaussian beams, multi-sinc Schell-model beams, sinc Schell-model pulses, twisted sinc-correlation Schell-model beams, and others [16-22].

Furthermore, the unified theory of coherent polarization has established a close connection between the coherence and polarization of light fields, offering a novel approach to comprehending optical statistical characteristics more comprehensively [23]. Based on this theory, theoretical and experimental investigations have been conducted on electromagnetic Gaussian Schell model (EM GSM) beams and electromagnetic special-correlated Schell-model beams [24-27]. The EM GSM beams exhibit advantages over scalar beams in mitigating turbulence-induced scintillation and ghosting. Correspondingly, electromagnetic Schell-model sources with a twisted phase have been extensively studied [28-30]. The research has revealed that the statistical properties of twisted EM beams are influenced by both the twisted phase and the degree of polarization of the source beam. The electromagnetic sinc-Schell model (EM SSM) beam also displays distinctive propagation characteristics distinct from those of the scalar sinc-Schell model beam. The statistical properties of electromagnetic sinc-Schell model vortex beams can maintain their vortex structures in the far field, depending on the topological charges and source parameters [31]. However, up to now, there has been a rare report on research on the EM SSM with a twisted correlation structure.

In this work, we expand the scalar twisted sinc-correlation Schell-model (TSSM) beam into the electromagnetic (EM) domain and establish the required source parameter conditions for generating a physically realizable beam. Using the extended Huygens–Fresnel principle, we derive the elements of the cross-spectral density (CSD) matrix for the beam propagating in free space and atmospheric turbulence. Our analysis focuses on investigating the impact of the twisted phase and correlated source parameters on the statistical properties of these beams, explicitly examining their spectral density, degree of polarization, and degree of coherence during propagation in atmospheric turbulence. Through detailed exploration, we have obtained valuable findings from these investigations.

## 2. EM TSSM source

The cross-spectral density (CSD) function can be used to describe the second-order correlation properties of a statistically EM TSSM source at a pair of points  $\rho_1$  and  $\rho_2$  in the source plane  $z = 0$ , as shown in previous research [24].

$$W_{\alpha\beta}(\rho_1, \rho_2) = \langle E_\alpha^*(\rho_1) E_\beta(\rho_2) \rangle, \quad (\alpha, \beta = x, y) \quad (1)$$

where  $E_x$  and  $E_y$  represent the two components of the random electric vector along the  $x$  and  $y$  axes, respectively, which are mutually orthogonal. The asterisk denotes the complex conjugate operation, and the angular brackets signify the average over a monochromatic ensemble.

As reported by GORI *et al.* [9, 10], the integral representation of the form mentioned above fulfills the non-negative definiteness requirements necessary for CSD matrices to be physically realizable.

$$W_{\alpha\beta}(\rho_1, \rho_2) = \int p_{\alpha\beta}(v) h_\alpha^*(\rho_1, v) h_\beta(\rho_2, v) dv \quad (2)$$

where  $p_{\alpha\beta}(v)$  is a non-negative function,  $v$  denotes a two-dimensional vector.  $h_\alpha(\rho_1, v)$  and  $h_\beta(\rho_2, v)$  represent arbitrary kernel functions. Each choice of them may lead to different classes of CSD matrix.

We adopt the following kernel function to generate vector sources with rotating intensity [9].

$$h_\alpha(\rho, v) = C_\alpha \exp\left[-\frac{\rho_x^2}{2\sigma_x^2} - \frac{\rho_y^2}{2\sigma_y^2}\right] \exp\left[-(u\rho_y + i\rho_x)v_x + (u\rho_x - i\rho_y)v_y\right] \quad (3)$$

where  $\rho_x$  and  $\rho_y$  are coordinate components on the source plane,  $v_x$  and  $v_y$  denote spacial frequency components, the beam width is denoted by  $\sigma_x$  and  $\sigma_y$ , respectively, while  $u$  represents the twist factor.  $C_\alpha$  represents the amplitudes of the electric field component along the  $\alpha$  direction. The function  $p_{\alpha\beta}(v)$  is given as follows [21]:

$$p_{\alpha\beta}(v) = C_{\alpha\beta} \frac{\delta_{\alpha\beta}^2}{\pi^2} \text{rect}\left(\frac{\delta_{\alpha\beta} v_x}{\pi}\right) \text{rect}\left(\frac{\delta_{\alpha\beta} v_y}{\pi}\right) \quad (4)$$

where  $\delta_{\alpha\beta}$  denotes coherence length, and  $C_{\alpha\beta}$  is the complex correlation coefficient,  $\text{rect}(\cdot)$  is the rectangular function, which equals 1 when  $x < 1/2$  and 0 otherwise. Here, the choice of function  $p_{\alpha\beta}(v)$  is to generate a correlation function related to the sinc function through the Fourier transform of the rectangular function. Substituting Eqs. (3) and (4) into Eq. (2), and applying the following integral formula:

$$\int f(x) \text{rect}(2\pi i v) dx = \text{Sinc}(x) \quad (5)$$

the cross-spectral density (CSD) of the EM TSSM beams can be obtained using the following expression:

$$W_{\alpha\beta}(\rho_1, \rho_2) = \int p_{\alpha\beta}(v) h_\alpha^*(\rho_1, v) h_\beta(\rho_2, v) dv \quad (6a)$$

and further

$$\begin{aligned}
 W_{\alpha\beta}(\rho_1, \rho_2) = & C_\alpha C_\beta C_{\alpha\beta} \exp\left(-\frac{\rho_{1x}^2 + \rho_{2x}^2}{2\sigma_x^2} - \frac{\rho_{1y}^2 + \rho_{2y}^2}{2\sigma_y^2}\right) \\
 & \times \text{Sinc}\left[\frac{(\rho_{1x} - \rho_{2x}) + iu(\rho_{1y} + \rho_{2y})}{2\delta_{\alpha\beta}}\right] \\
 & \times \text{Sinc}\left[\frac{(\rho_{1y} - \rho_{2y}) + iu(\rho_{1x} + \rho_{2x})}{2\delta_{\alpha\beta}}\right]
 \end{aligned} \tag{6b}$$

In order to ensure the physical realizability of the field described in Eq. (6), certain constraints on the source parameters need to be established. Consequently, the CSD matrices must be quasi-Hermitian [10], meaning that  $W_{\alpha\beta}(\rho_1, \rho_2) = W_{\beta\alpha}(\rho_1, \rho_2)$ . It is sufficient for this condition to be satisfied if

$$C_{xx} = C_{yy} = 1, \quad |C_{xy}| = |C_{yx}|, \quad \delta_{yx} = \delta_{xy} \tag{7}$$

Moreover, the requirement of non-negative definiteness for genuine CSD matrices results in the following set of inequalities.

$$p_{\alpha\alpha}(v) \geq 0, \quad p_{xx}(v) \cdot p_{yy}(v) - p_{xy}(v) \cdot p_{yx}(v) \geq 0 \tag{8}$$

must be met for any  $v$ . By examining Eq. (4), it becomes evident that inequality (8) is always satisfied. Substituting Eq. (4) into the inequalities (8), we can derive the following set of inequality relations.

$$\delta_{xx}^2 \delta_{yy}^2 \text{rect}\left(\frac{\delta_{xx} v}{\pi}\right) \cdot \text{rect}\left(\frac{\delta_{yy} v}{\pi}\right) \geq |C_{xy}|^2 \delta_{xy}^2 \left[ \text{rect}\left(\frac{\delta_{xy} v}{\pi}\right) \right]^2 \tag{9}$$

According to the definition of the rectangular function, we can determine that the following fork inequality serves as the condition for realizability.

$$\max\{\delta_{xx}, \delta_{yy}\} \leq \delta_{xy} \leq \frac{\sqrt{\delta_{xx} \delta_{yy}}}{|C_{xy}|} \tag{10}$$

### 3. The CSD matrix of the EM TSSM sources in a linear random medium

Assume the source in Eq. (6) produces a beam-like field propagating into a turbulent atmosphere-filled half-space with  $z > 0$ . The extended Huygens–Fresnel integral can be described by the paraxial propagation of the CSD of the EM TSSM beams.

$$W_{\alpha\beta}(r_1, r_2, z) = \left(\frac{k}{2\pi z}\right)^2 \int \int \left\{ W_{\alpha\beta}(\rho_1, \rho_2) \exp\left[-ik\frac{(r_1 - \rho_1)^2 - (r_2 - \rho_2)^2}{2z}\right] \times \langle \exp[\psi(r_1, \rho_1) + \psi^*(r_2, \rho_2)] \rangle_R \right\} d\rho_1 d\rho_2 \quad (11)$$

where  $k = 2\pi/\lambda$  is spacial wave number,  $\lambda$  is wavelength,  $r_1$  and  $r_2$  are two points in the observation plane of propagation distance  $z$ ,  $\psi$  stands for the complex phase perturbation caused by the medium,  $\langle \cdot \rangle_R$  implying averaging over the ensemble of statistical realizations of the turbulence. Under quadratic phase approximations,  $\langle \cdot \rangle_R$  can be re-written as

$$\begin{aligned} & \langle \exp[\psi(r_1, \rho_1) + \psi^*(r_2, \rho_2)] \rangle_R \\ &= \exp\left\{-\frac{\pi^2 k^2 z}{3} \int_0^\infty \kappa^3 \Phi_n(\kappa) d\kappa \left[ (r_1 - r_2)^2 + (r_1 - r_2)(\rho_1 - \rho_2) + (\rho_1 - \rho_2)^2 \right]\right\} \end{aligned} \quad (12)$$

Here, we select the van Karman power spectrum to represent the anisotropic characteristics of the atmosphere [7, 17], where  $\kappa$  represents the magnitude of the spatial wave number.

$$\Phi_n(\kappa) = 0.033 C_n^2 (\kappa^2 + \kappa_0^2)^{-11/6} \exp(\kappa^2 / \kappa_m) \quad (13)$$

where  $C_n^2$  represents a generalized refractive-index structure parameter,  $\kappa_0 = 2\pi/L_0$  and  $\kappa_m = 5.92/l_0$  with  $L_0$  and  $l_0$  represent parameters associated with the outer scale and inner scale of turbulence, respectively. By substituting equations (2) and (12) into equation (11) and performing mathematical calculations, we can derive the following expression

$$\begin{aligned} W_{\alpha\beta}(r_1, r_2, z) &= \frac{C_\alpha C_\beta C_{\alpha\beta} k^2}{4z^2 \sqrt{(a_x a_y c_x c_y)^*}} \exp\left[\frac{ik}{2z} (r_2^2 - r_1^2) + i(r_2^2 - r_1^2)\right] \\ &\times \int \int p_{\alpha\beta}(v) h(v_x, v_y) dv_x dv_y \end{aligned} \quad (14)$$

with

$$\begin{aligned} h(v_x, v_y) &= \exp\left\{\frac{1}{4a_x^*} \left[ F_1(x_1, x_2) - uv_y + iv_x \right]^2 + \frac{1}{4b_x} \left[ F_2(x_1, x_2) + ud_x v_y + ie_x v_x \right]^2\right\} \\ &\times \exp\left\{\frac{1}{4a_y^*} \left[ F_1(y_1, y_2) + uv_x + iv_y \right]^2 + \frac{1}{4b_y} \left[ F_2(y_1, y_2) - ud_y v_x + ie_y v_y \right]^2\right\} \end{aligned} \quad (15)$$

where

$$\begin{aligned} F_1(\alpha_1, \alpha_2) &= \frac{ik\alpha_2}{z} - t(\alpha_2 - \alpha_1), \\ F_2(\alpha_1, \alpha_2) &= \frac{ik}{z} \left( \alpha_1 + \frac{t}{b_{1\alpha}^*} \alpha_2 \right) + c_\alpha (\alpha_1 - \alpha_2), \quad (\alpha = x, y) \end{aligned} \quad (16)$$

$$\begin{aligned} a_\alpha &= \frac{1}{\sigma_\alpha} + \frac{ik}{2z} - t, \quad b_\alpha = a_\alpha + \frac{t^2}{a_\alpha^*}, \quad c_\alpha = t \left( 1 + \frac{t}{a_\alpha^*} \right), \\ d_\alpha &= 1 - \frac{t}{a_\alpha^*}, \quad e_\alpha = 1 + \frac{t}{a_\alpha^*}, \quad (\alpha = x, y) \end{aligned} \quad (17)$$

$$t = \frac{4\pi^2 k^2 z^2}{3} \int \kappa^3 \Phi_n(\kappa) d^2 \kappa \quad (18)$$

By analyzing equations (14)–(18), we can calculate the cross-spectral density (CSD) matrix of the EM TSSM beam at any propagation distance. When  $r_1 = r_2 = r$ , the spectral density for the EM TSSM beam can be obtained from the given expression

$$S(r, z) = W_{xx}(r, r, z) + W_{yy}(r, r, z) \quad (19)$$

The DOP and DOC of the EM TSSM beams can be estimated using the formula

$$P(r, z) = \sqrt{1 - \frac{4 \text{Det}[W(r, r, z)]}{\left\{ \text{Tr}[W(r, r, z)] \right\}^2}} \quad (20)$$

$$\mu(r_1, r_2, z) = \frac{\text{Tr}[W(r_1, r_2, z)]}{\sqrt{\text{Tr}[W(r_1, r_1, z)] \cdot \text{Tr}[W(r_2, r_2, z)]}} \quad (21)$$

where Det and Tr denote the matrix's determinant and trace, we can analyze the properties in free space and turbulent atmosphere by applying Eqs. (19)–(21).

#### 4. Numerical simulation and analysis

In this section, we present a series of numerical examples to demonstrate the propagation characteristics of the EM TSSM beam in both free space and a turbulent atmosphere. For the sake of simplicity, we assume certain initial parameter values for

the EM TSSM beams and turbulence. Specifically, we set  $C_x = C_y = 1$ ,  $|C_{xy}| = 0.2$ ,  $\lambda = 632.8$  nm,  $\delta_x = 1$  mm,  $\delta_y = 1.5$  mm,  $\delta_{xy} = 1.5$  mm,  $\sigma_x = 10$  mm,  $\sigma_y = 10$  mm,  $L_0 = 1$  m, and  $l_0 = 1$  mm, unless stated otherwise in the figure captions.

Figure 1 illustrates the spectral density evolution of the EM TSSM beam at various twist factor values in the transverse plane during propagation in free space. Subfigures (a1)–(d1) in Fig. 1 depict the spectral density distribution of the EM SSM beam ( $u = 0$ ), showing a Gaussian profile at the source plane that gradually transforms into a flat top distribution as it propagates. The distribution scale increases with the propagation distance. Subfigures (a2)–(d2) and (a3)–(d3) in Fig. 1 present the spectral density evolution of the EM TSSM beam at twist factor values  $u = -2$  and  $u = 2$ , respectively.

We can find that the twist factor induces two significant effects on the spectral density. Firstly, it causes a 90-degree rotation of the spectral density, with a clockwise rotation for  $u > 0$  and a counterclockwise rotation for  $u < 0$ . Secondly, the twist factor leads to a self-splitting spectral density distribution, resulting from the rotation of the twisted phase factor and sinc correlation function due to the Fourier transform of the rectangular function. This phenomenon causes the beam to self-split during propagation. As observed in Fig. 1, the light spots gradually expand and split into a  $2 \times 2$  isotropic array as they propagate, contrasting with the evolution from Gaussian to flat profile observed in (a1)–(d1). Where the beams gradually change from a Gaussian profile to a flat profile with increasing propagation distance.

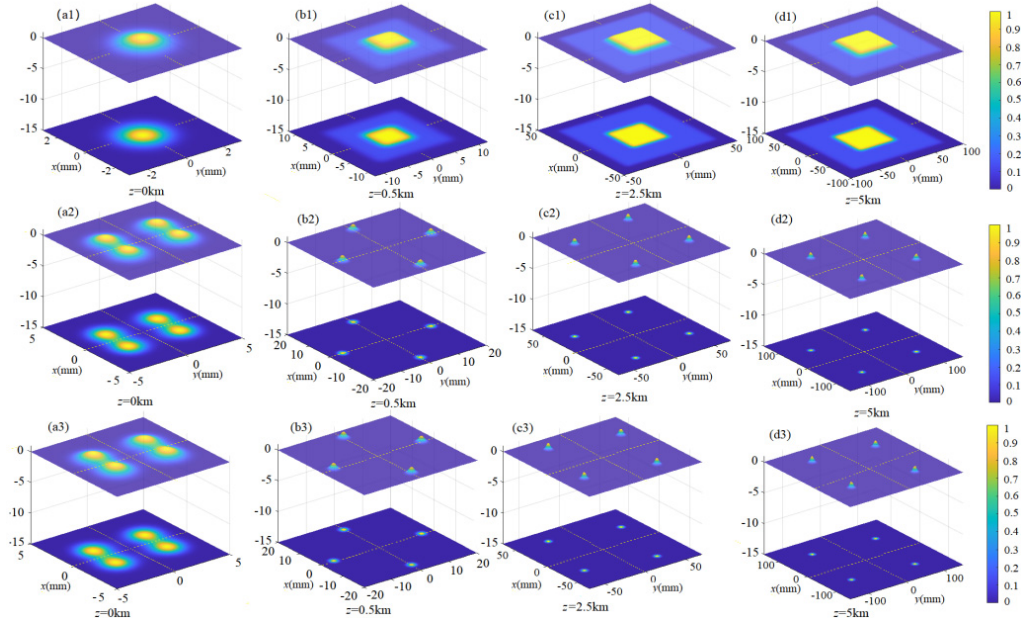


Fig. 1. The normalized spectral density of the EM TSSM beams at varying distances in free space. The figures include (a1)–(d1) with  $u = 0$ , (a2)–(d2) with  $u = -2$ , and (a3)–(d3) with  $u = 2$ .

Figure 2 shows the spectral intensity distribution of the EM TSSM beams for various twisted factor values propagating in atmospheric turbulence. Unlike the sinc Schell -model beam without the twisted phase in Fig. 2 (a1)–(d1), its spectral intensity

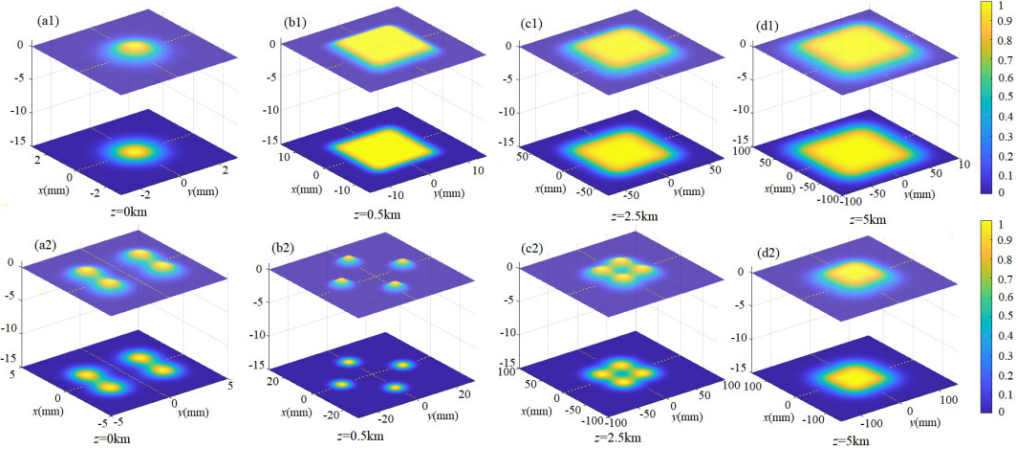


Fig. 2. The normalized spectral density of the EM TSSM beams at varying distances in the atmospheric turbulence. The figures include (a1)–(d1) with  $u = 0$ , (a2)–(d2) with  $u = -2$ .

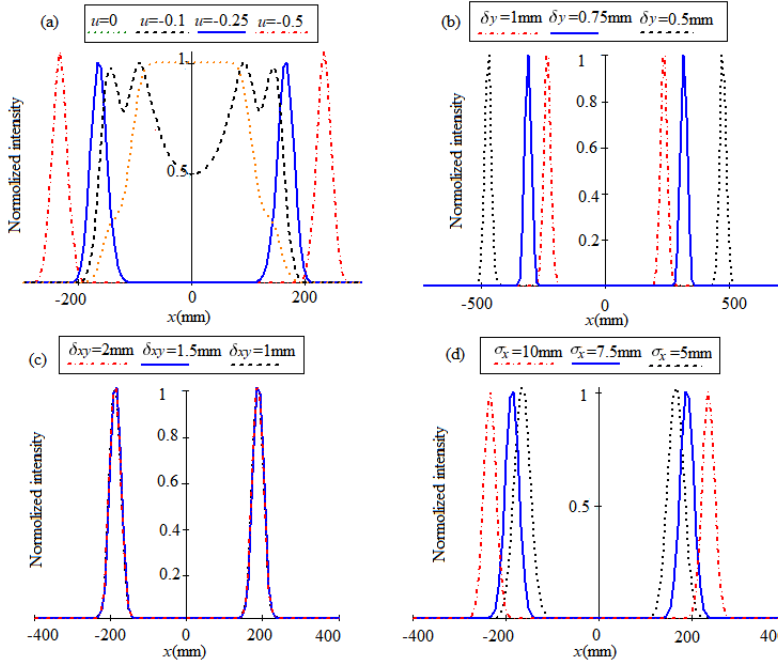


Fig. 3. The normalized spectral density of the EM TSSM beams with  $C_n^2 = 10^{-18} \text{ m}^{-2/3}$  at transmission distance  $z = 1 \text{ km}$  for varying beam parameters in atmospheric turbulence. (a)  $\delta_{xy} = 2 \text{ mm}$ ; (b)  $u = -0.5$ ,  $\delta_{xy} = 2 \text{ mm}$ ; (c)  $u = -0.5$ ; (d)  $u = -0.5$ ,  $\delta_{xy} = 2 \text{ mm}$ .

evolves a flat-top distribution. In Fig. 2 (a2)–(d2), with increasing propagation distances, the array of the EM TSSM beam converges inward, gradually combining into the flat-top distribution while maintaining rotation.

Figure 3 exhibits the spectral density evolution of the EM TSSM beam with different initial beam parameters propagating in atmospheric turbulence. Specifically, the analysis focuses on the  $y = 0$  plane at a propagation distance of  $z = 1$  km for simplicity. Figure 3(a) highlights the significant role of the twist factor in splitting the light spot. As the twist factor values increase, the spectral intensity starts to sink from a flat-top distribution. It gradually splits into two peaks, moving outward along the  $x$ -axis, with the spacing between the peaks gradually widening. This outcome indicates the formation of a stable beam array influenced by the twist factor, offering effective control over the array distribution by adjusting the beam parameters. Figure 3(b)–(d) demonstrates that the coherence length  $\delta_y$  and beam width  $\sigma_x$  also impact the peak shift, while the coherence length  $\delta_{xy}$  does not affect the peak shift.

Next, we focus on the variations of the DOP of the EM TSSM beam. As shown in Fig. 4, the DOP distribution of the EM TSSM beams at various transmission distances in free space is shown. We can see that, whether it is an EM SSM beam or an EM TSSM beam, the distribution of DOP on the source plane is uniform, and the value of the DOP depends on the selection of source parameters. As the transmission distance increases, a rectangular depression area with multiple peaks gradually forms in the distribution center, and the scope of the depression increases. Furthermore, the DOP distribution of the EM TSSM beams (as depicted in Fig. 4(b)) demonstrates rotation, with the direction of rotation closely tied to the twist factor. When the twist factor is positive, the DOP distribution exhibits a clockwise rotation, while a negative twist factor results in an anticlockwise rotation.

Figure 5 shows the DOP distribution of the EM TSSM beam for different propagation distances in atmospheric turbulence. Compared with the distribution in free space, we can find that, for the EM SSM beams, the scale of non-uniform DOP distribution becomes smaller due to the influence of turbulence. However, for EM TSSM beams,

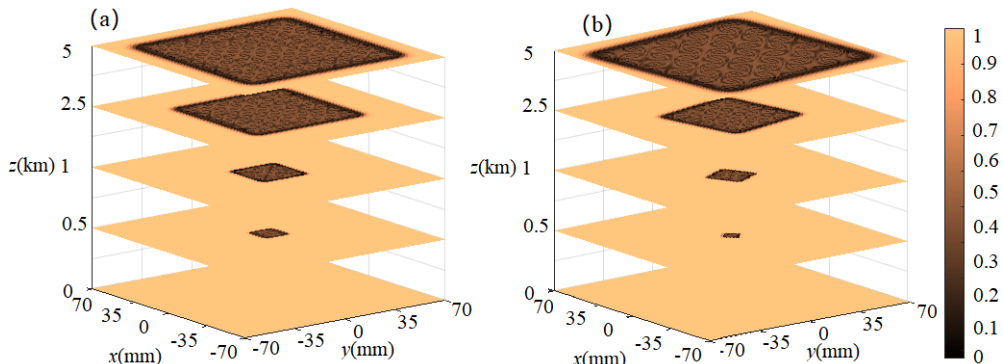


Fig. 4. The distribution of spectral degree of polarization of the EM TSSM beams at varying transmission distances in free space. The figures includes (a) with  $u = 0$ , (b) with  $u = -0.5$ .

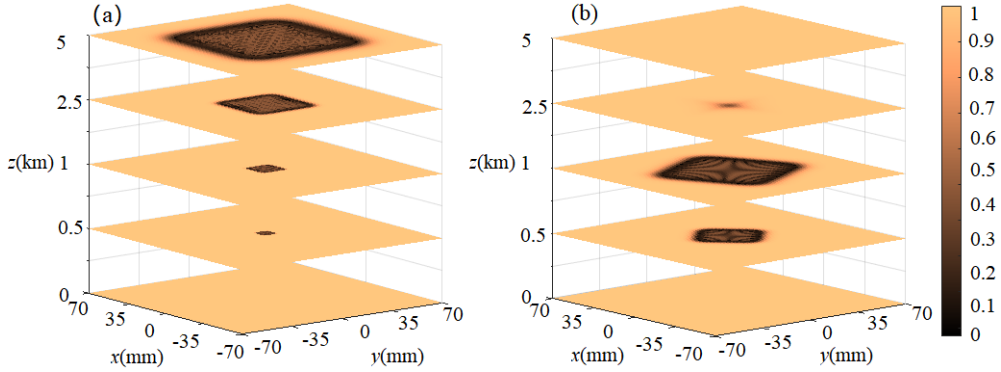


Fig. 5. The distribution of spectral degree of polarization of the EM TSSM beams at varying transmission distances in atmospheric turbulence. The figures include (a) with  $u = 0$ , (b) with  $u = -0.5$ .

the size of the non-uniform DOP distribution rapidly increases at first and then gradually decreases. When the beam transmits to a certain distance, the non-uniform distribution area disappears, and the DOP distribution returns to its original uniform distribution. It indicates that the EM TSSM beams can automatically restore their degree of polarization in atmospheric turbulence.

Figure 6 illustrates the impact of the twist factor, beam length, and coherence length on the DOP of the EM TSSM beam with various beam parameters along the  $x$ -axis

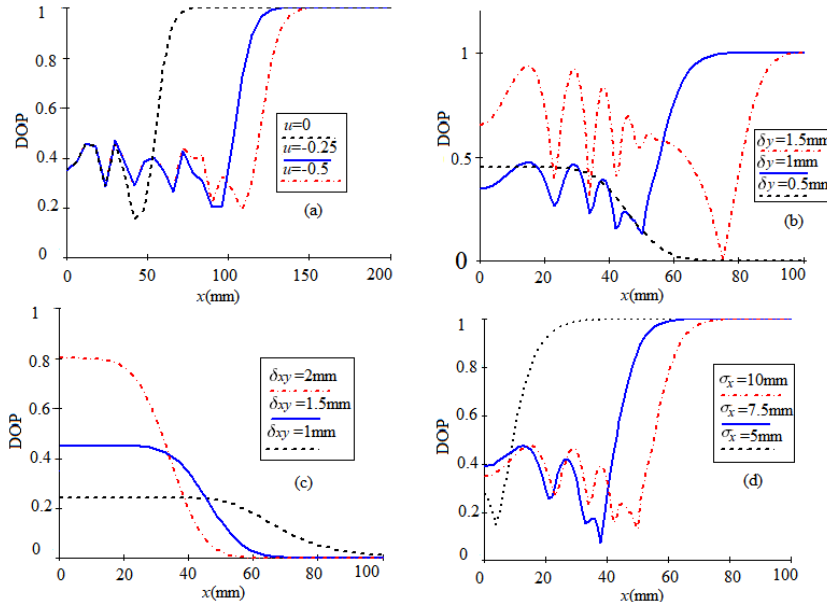


Fig. 6. The distribution of spectral degree of polarization of the EM TSSM beam with  $C_n^2 = 10^{-18} \text{ m}^{-2/3}$  at transmission distance  $z = 0.5 \text{ km}$  for varying beam parameters in the atmospheric turbulence. (a)  $u = 0$ ,  $\delta_{xy} = 2 \text{ mm}$ ; (b)  $u = -0.5$ ,  $\delta_{xy} = 2 \text{ mm}$ ; (c)  $u = -0.5$ ; (d)  $u = -0.5$ ,  $\delta_{xy} = 2 \text{ mm}$ .

at  $z = 0.5$  km in atmospheric turbulence. The DOP initially fluctuates and oscillates along the  $x$ -axis, forming multiple peaks and finally approaching a stable value. In addition, different beam parameters have different effects on the DOP distribution of the EM TSSM beam.

Finally, we will examine the DOC (degree of coherence) behavior of the EM TSSM beam by studying the relationship between  $x = x_2 - x_1$  and  $y = y_2 - y_1$ , where  $x_1 = -x_2 = -x/2$  and  $y_1 = -y_2 = -y/2$  for two points relative to the optical axis. Figure 7 illustrates the DOC evolution of the EM TSSM beam with  $u = -0.5$  for varying transmission distances in free space. It can be found that, with increased transmission distance, the DOC gradually changes from a Gaussian distribution to a grid-shaped strip distribution, rotating counterclockwise around its central region. However, as the transmission distance increases beyond a particular value, the rotation direction reverses and becomes clockwise. After a certain transmission distance, it returns to a counterclockwise rotation until it reaches 90 degrees. Subsequently, its distribution remains unchanged in shape except for increasing the scale.

Figure 8 presents the DOC distribution of the EM TSSM beam at a transmission distance of  $z = 0.5$  km for various atmospheric parameter values. As atmospheric parameters increase, the DOC distribution area gradually increases as the transmission

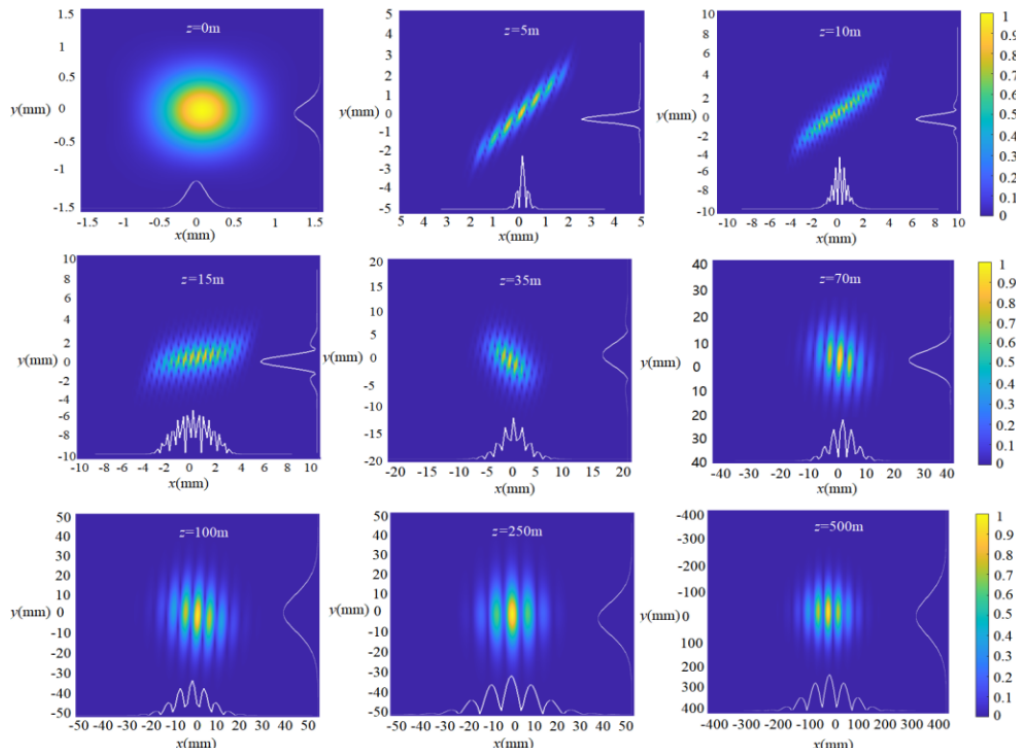


Fig. 7. The distribution of the degree of spectral coherence of the EM TSSM beam with  $u = -0.5$  at varying transmission distances in free space.

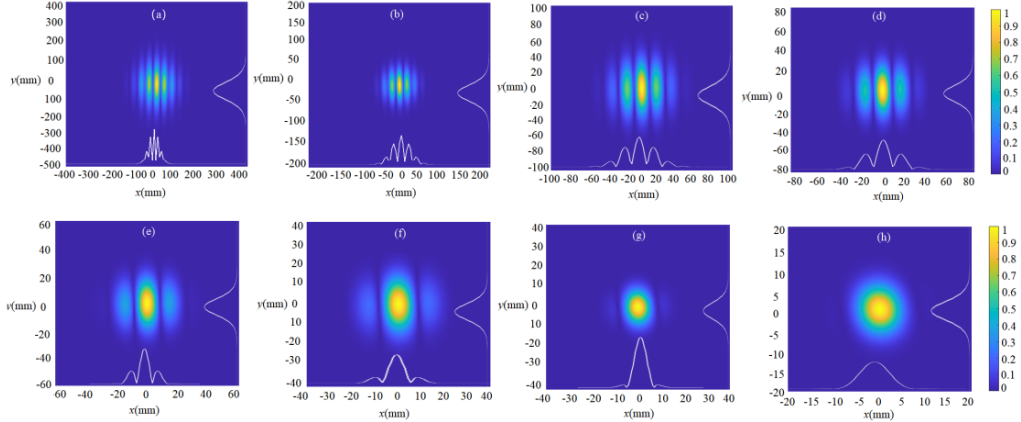


Fig. 8. The distribution of the degree of spectral coherence of the EM TSSM beams at transmission distance  $z = 0.5$  km for varying values of atmosphere parameters. (a)  $C_n^2 = 0$ ; (b)  $C_n^2 = 10^{-19} \text{ m}^{-2/3}$ ; (c)  $C_n^2 = 2 \times 10^{-19} \text{ m}^{-2/3}$ ; (d)  $C_n^2 = 5 \times 10^{-19} \text{ m}^{-2/3}$ ; (e)  $C_n^2 = 10^{-18} \text{ m}^{-2/3}$ ; (f)  $C_n^2 = 2 \times 10^{-18} \text{ m}^{-2/3}$ ; (g)  $C_n^2 = 5 \times 10^{-18} \text{ m}^{-2/3}$ ; (h)  $C_n^2 = 10^{-17} \text{ m}^{-2/3}$ .

distance increases, and the number of bars in the distribution area decreases. The DOC distribution eventually evolves into a Gaussian-like distribution.

Figure 9 illustrates the variation curves of the DOC of the EM TSSM beam with various beam parameters along the  $x$ -axis at  $z = 0.5$  km in atmospheric turbulence. We

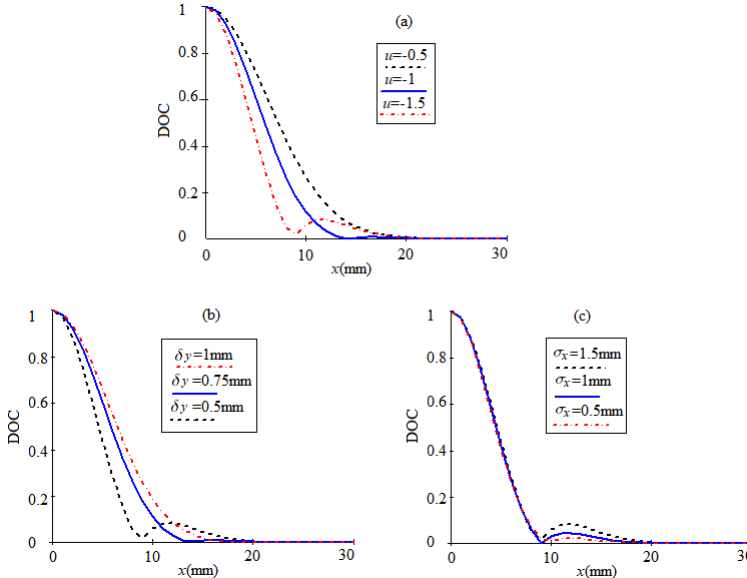


Fig. 9. The distribution of the degree of spectral coherence of the EM TSSM beams with  $C_n^2 = 2 \times 10^{-18} \text{ m}^{-2/3}$  at transmission distance  $z = 0.5$  km for varying beam parameters in the atmospheric turbulence. (a)  $\delta_x = 1 \text{ mm}$ ,  $\delta_y = 0.5 \text{ mm}$ ; (b)  $u = -0.5$ ,  $\delta_x = 1 \text{ mm}$ ; (c)  $u = -0.5$ ,  $\delta_x = 1 \text{ mm}$ ,  $\delta_y = 1.5 \text{ mm}$ .

can see that as the twist factor  $u$  decreases or the correlation length  $\delta_y$  increases (see Fig. 9(a) and (b)), the distribution range of DOC gradually expands, while the beam width  $\sigma_x$  only affects the distribution of the side lobes of DOC without affecting the main lobe distribution of the DOC.

## 5. Conclusion

This study introduces the concept of a twisted electromagnetic sinc-correlation Schell-model (EM TSSM) beam and examines the necessary conditions for generating such a beam. Several numerical examples are used to analyze the impact of source characteristics and turbulent parameters on the statistical properties of these beams during propagation. A twisted phase in these beams leads to rotational and self-splitting intensity profiles, allowing them to maintain their shape in free space and turbulent atmospheres. Compared to sinc Schell-model beams without the twisted phase, the DOP distribution of EM TSSM beams can exhibit rotation around its center. Moreover, in a turbulent atmosphere, these beams can exhibit self-healing of their DOP distribution within specific propagation ranges. The twist factor introduces non-unidirectional rotation of the DOC distribution in free space, which evolves from multi-strip profiles to a Gaussian-like distribution in atmospheric turbulence. Additionally, the beam parameters play a significant role in shaping the DOC. The findings of this study hold potential benefits for applications such as optical trapping and optical communication.

### Funding

National Science Foundation of China (12265018).

### Conflict of interest

The authors declare no conflict of interest.

## References

- [1] GBUR G., *Partially coherent beam propagation in atmospheric turbulence*, Journal of the Optical Society of America A **31**(9), 2014: 2038-2045. <https://doi.org/10.1364/JOSAA.31.002038>
- [2] CAI Y., CHEN Y., YU J., LIU X., LIU L., *Chapter Three - Generation of Partially Coherent Beams*, Progress in Optics, Vol. 62, 2017: 157-223. <https://doi.org/10.1016/bs.po.2016.11.001>
- [3] GBUR G., WOLF E., *Spreading of partially coherent beams in random media*, Journal of the Optical Society of America A **19**(8), 2002: 1592-1598. <https://doi.org/10.1364/JOSAA.19.001592>
- [4] SHIRAI T., DOGARIU A., WOLF E., *Mode analysis of spreading of partially coherent beams propagating through atmospheric turbulence*, Journal of the Optical Society of America A **20**(6), 2003: 1094-1102. <https://doi.org/10.1364/JOSAA.20.001094>
- [5] KOROTKOVA O., SAHIN S. AND SHCHEPAKINA E., *Multi-Gaussian Schell-model beams*, Journal of the Optical Society of America A **29**(10), 2012: 2159-2164. <https://doi.org/10.1364/JOSAA.29.002159>
- [6] MEI Z., KOROTKOVA O., *Random sources generating ring-shaped beams*, Optics Letters **38**(2), 2013: 91-93. <https://doi.org/10.1364/OL.38.000091>
- [7] CHEN Y., GU J., WANG F., CAI Y., *Self-splitting properties of a Hermite-Gaussian correlated Schell-model beam*, Physical Review A **91**(1), 2015: 013823. <https://doi.org/10.1103/PhysRevA.91.013823>

- [8] LIANG C., WANG F., LIU X., CAI Y., KOROTKOVA O., *Experimental generation of cosine-Gaussian-correlated Schell-model beams with rectangular symmetry*, Optics Letters **39**(4), 2014: 769-772. <https://doi.org/10.1364/OL.39.000769>
- [9] GORI F., SANTARSIERO M., *Devising genuine spatial correlation functions*, Optics Letters **32**(24), 2007: 3531-3533. <https://doi.org/10.1364/OL.32.003531>
- [10] GORI F., RAMÍREZ-SÁNCHEZ V., SANTARSIERO M., SHIRAI T., *On genuine cross-spectral density matrices*, Journal of Optics A: Pure and Applied Optics **11**(8), 2009: 085706. <https://doi.org/10.1088/1464-4258/11/8/085706>
- [11] MAO H., CHEN Y., LIANG C., CHEN L., CAI Y., PONOMARENKO S.A., *Self-steering partially coherent vector beams*, Optics Express **27**(10), 2019: 14353-14368. <https://doi.org/10.1364/OE.27.014353>
- [12] YU J., CHEN Y., LIU L., LIU X., CAI Y., *Splitting and combining properties of an elegant Hermite-Gaussian correlated Schell-model beam in Kolmogorov and non-Kolmogorov turbulence*, Optics Express **23**(10), 2015: 13467-13481. <https://doi.org/10.1364/OE.23.013467>
- [13] CHEN Y., CAI Y., *Generation of a controllable optical cage by focusing a Laguerre-Gaussian correlated Schell-model beam*, Optics Letters **39**(9), 2014: 2549-2552. <https://doi.org/10.1364/OL.39.002549>
- [14] MEI Z., *Light sources generating self-focusing beams of variable focal length*, Optics Letters **39**(2), 2014: 347-350. <https://doi.org/10.1364/OL.39.000347>
- [15] MEI Z., *Two types of Sinc Schell-model beams and their propagation characteristics*, Optics Letters **39**(14) 2014: 4188-4191. <https://doi.org/10.1364/OL.39.004188>
- [16] MEI Z., MAO Y., *Electromagnetic sinc Schell-model beams and their statistical properties*, Optics Express **22**(19), 2014: 22534-22546. <https://doi.org/10.1364/OE.22.022534>
- [17] BAYRAKTAR M., DENIZ BASDEMIR H., *Cylindrical-sinc beam*, Optik **125**(19), 2014: 5869-5871. <https://doi.org/10.1016/j.ijleo.2014.07.054>
- [18] DING C., KOROTKOVA O., ZHANG Y., PAN L., *Sinc Schell-model pulses*, Optics Communications **339**, 2015: 115-122. <https://doi.org/10.1016/j.optcom.2014.11.074>
- [19] MEI Z., MAO Y., *Multi-sinc Schell-model beams and the interaction with a linear random medium*, Laser Physics Letters **12**(9), 2015: 095002. <https://doi.org/10.1088/1612-2011/12/9/095002>
- [20] ZHOU Y., ZHU W., ZHAO D., *Twisted sinc-correlation Schell-model beams*, Optics Express **30**(2), 2022: 1699-1707. <https://doi.org/10.1364/OE.450254>
- [21] LIU X., ZHOU G., SHEN Y., *Effect of oceanic turbulence with anisotropy on the propagation of multi-sinc Schell-model beams*, Results in Physics **36**, 2022: 105447. <https://doi.org/10.1016/j.rinp.2022.105447>
- [22] BAYRAKTAR M., *Scintillation and bit error rate analysis of cylindrical-sinc Gaussian beam*, Physica Scripta **95**(11), 2020: 115501. <https://doi.org/10.1088/1402-4896/abb0d0>
- [23] WOLF E., *Unified theory of coherence and polarization of random electromagnetic beams*, Physics Letters A **312**(5-6), 2003: 263-267. [https://doi.org/10.1016/S0375-9601\(03\)00684-4](https://doi.org/10.1016/S0375-9601(03)00684-4)
- [24] GORI F., SANTARSIERO M., BORGHI R., RAMÍREZ-SÁNCHEZ V., *Realizability condition for electromagnetic Schell-model sources*, Journal of the Optical Society of America A **25**(5), 2008: 1016-1021. <https://doi.org/10.1364/JOSAA.25.001016>
- [25] MEI Z., KOROTKOVA O., SHCHEPAKINA E., *Electromagnetic multi-Gaussian Schell-model beams*, Journal of Optics **15**(2), 2013: 025705. <https://doi.org/10.1088/2040-8978/15/2/025705>
- [26] TONG Z., KOROTKOVA O., *Electromagnetic nonuniformly correlated beams*, Journal of the Optical Society of America A **29**(10), 2012: 2154-2158. <https://doi.org/10.1364/JOSAA.29.002154>
- [27] MEI Z., KOROTKOVA O., *Electromagnetic cosine-Gaussian Schell-model beams in free space and atmospheric turbulence*, Optics Express **21**(22), 2013: 27246-27259. <https://doi.org/10.1364/OE.21.027246>
- [28] CAI Y., KOROTKOVA O., *Twist phase-induced polarization changes in electromagnetic Gaussian Schell-model beams*, Applied Physics B **96**, 2009: 499-507. <https://doi.org/10.1007/s00340-009-3469-0>
- [29] ZHU S., CAI Y., *Spectral shift of a twisted electromagnetic Gaussian Schell-model beam focused by a thin lens*, Applied Physics B **99**, 2010: 317-323. <https://doi.org/10.1007/s00340-010-3906-0>

- [30] LIU L., HUANG Y., CHEN Y., GUO L., CAI Y., *Orbital angular moment of an electromagnetic Gaussian Schell-model beam with a twist phase*, Optics Express **23**(23), 2015: 30283-30296. <https://doi.org/10.1364/OE.23.030283>
- [31] MEI Z., WANG Y., MAO Y., *Electromagnetic sinc Schell-model vortex beams*, IEEE Photonics Journal **11**(1), 2019: 6100308. <https://doi.org/10.1109/JPHOT.2018.2885012>

*Received May 23, 2023  
in revised form July 13, 2023*